

## Polarization Control in Three-Dimensional Resonant Coherent Excitation

Y. Nakano,<sup>1,\*</sup> C. Kondo,<sup>1,2,3</sup> A. Hatakeyama,<sup>2,4</sup> Y. Nakai,<sup>5</sup> T. Azuma,<sup>1</sup> K. Komaki,<sup>2,3</sup> Y. Yamazaki,<sup>2,3</sup>  
E. Takada,<sup>6</sup> and T. Murakami<sup>6</sup>

<sup>1</sup>Department of Physics, Tokyo Metropolitan University, Hachioji, Tokyo 192-0397, Japan

<sup>2</sup>Graduate School of Arts and Sciences, University of Tokyo, Komaba, Meguro, Tokyo 153-8902, Japan

<sup>3</sup>Atomic Physics Laboratory, RIKEN, Wako, Saitama 351-0198, Japan

<sup>4</sup>Department of Applied Physics, Tokyo University of Agriculture and Technology, Koganei, Tokyo 184-8588, Japan

<sup>5</sup>Radioactive Isotope Physics Laboratory, RIKEN Nishina Center, Wako, Saitama 351-0198, Japan

<sup>6</sup>National Institute of Radiological Sciences, Inage, Chiba 263-8555, Japan

(Received 14 October 2008; published 27 February 2009)

We present an experimental demonstration of an ingenious technique to control the alignment of the atomic internal state in the x-ray region using a periodic crystal field. The alignment directions of Ar<sup>16+</sup> and Fe<sup>24+</sup> ions were readily controlled by selecting the array of atomic planes using three-dimensional resonant coherent excitation, and were probed via the anisotropy of the deexcitation x-ray emission. We applied this method to a double resonance experiment, and succeeded in controlling the population of the specific magnetic substate in a  $\Lambda$ -type three-level configuration.

DOI: 10.1103/PhysRevLett.102.085502

PACS numbers: 61.85.+p, 32.90.+a, 34.50.Fa

Polarized light allows one to probe or manipulate the population of specific magnetic substates of atomic internal states. Optical pumping of atoms using laser technology is now an indispensable technique in atomic physics research. Deep insight into atomic collisional processes involving atoms, molecules, electrons, and photons is gained by the optical preparation of aligned materials [1]. In this Letter, we demonstrate the three-dimensional alignment of highly charged heavy ions traveling through a thin Si crystal, accompanied by an electronic transition in the x-ray energy region. We resonantly excited the heavy ions using the periodic crystal field instead of the light field, which is called resonant coherent excitation (RCE) [2–8]. In three-dimensional resonant coherent excitation (3D-RCE), a novel type of RCE induced by a periodic array of atomic planes [9], the ions experience a linearly polarized oscillating field in the crystal. We observed the deexcitation x-ray emission from ions excited through 3D-RCE for the first time, and found a distinct angular anisotropy that depended on the polarization direction of the oscillating crystal field.

RCE has often been observed under particular incident conditions where the ions travel in open spaces (channels) surrounded by atomic strings (axial channeling) or planes (planar channeling) in the crystal. Under these conditions, the ions experience not only an oscillating field but also a static field, and both are heavily dependent on their transverse position in the channel, i.e., the distance from the channel center [5]. The clear observation of alignment is prevented by this trajectory dependence in the direction and amplitude of the oscillating field as well as the strength of the static field that induces the static Stark effect, except in some particular cases [10–12]. In contrast, RCE under nonchanneling conditions, i.e., 3D-RCE, is characterized

by the trajectory independence of the oscillating field, and is inherently free from the static Stark effect [9]. Consequently, 3D-RCE is regarded as an ideal tool for controlling the alignment of the fast ions in a crystal.

Figure 1(a) shows the configuration of the ion trajectory in a Si crystal, where  $\mathbf{A} = (-1, 1, 0)a/2$ ,  $\mathbf{B} = (0, 0, 1)a$ , and  $\mathbf{C} = (1, 1, 0)a/2$  ( $a$ : lattice constant) are the base lattice vectors. The incident velocity  $\mathbf{v}$  and the two incident angles,  $\theta$  and  $\phi$ , characterize the periodic interaction between the ions and the crystal. The  $z$  axis is taken to be parallel to the ion beam and  $x$  and  $y$  axes orthogonal to  $z$ , so that the directions of  $(x, y, z)$  and  $(-\mathbf{C}, \mathbf{B}, \mathbf{A})$  coincide when  $\theta = \phi = 0$ . An array of atomic planes is specified by the reciprocal lattice vector defined by  $\mathbf{g}_{k,l,m} = k\mathbf{A}^* + l\mathbf{B}^* + m\mathbf{C}^*$ , with the Miller index  $(k, l, m)$ , and the base vectors  $\mathbf{A}^* = (-1, 1, 0)/a$ ,  $\mathbf{B}^* = (0, 0, 1)/a$ , and  $\mathbf{C}^* = (1, 1, 0)/a$ . The periodic electric field in the crystal at a position  $\mathbf{r}$  is given by  $\mathbf{F}(\mathbf{r}) = \sum_{\mathbf{g}} \mathbf{F}_{\mathbf{g}} \exp(-2\pi i \mathbf{g} \cdot \mathbf{r})$  as a summation of the plane waves, where  $\mathbf{F}_{\mathbf{g}} = 2\pi i \mathbf{g} V_{\mathbf{g}}$ ,

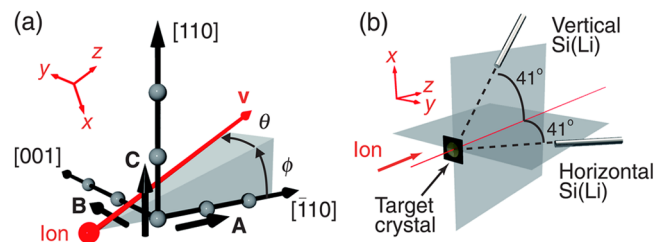


FIG. 1 (color online). (a) Orthogonal coordinate system of a Si crystal.  $\theta$  and  $\phi$  are the ion incident angles with respect to the  $[\bar{1}10]$  axis. (b) Schematic layout of the experimental setup. Two Si(Li) x-ray detectors were installed in the horizontal and vertical planes. The target crystal was mounted on a high-precision three-axis goniometer.

being the Fourier coefficient of the scalar potential. Each component is polarized parallel to  $\mathbf{g}$ , i.e., normal to the corresponding atomic planes. Because the ion position in the crystal at time  $t$  can be given by  $\mathbf{r} = \mathbf{v}t$  ( $\mathbf{v}$ : ion velocity) under the nonchanneling condition, it is obvious that the ions experience *trajectory-independent* plane waves without static components of the crystal fields. Note that the static field arising from the electronic stopping (wake field) is weak ( $\sim 1$  V/Å), and the effect on the ion motion or internal states is negligible. Taking into account the Lorentz transformation, the oscillating frequency in the ion rest frame is represented by  $\gamma\mathbf{g} \cdot \mathbf{v}$ , leading to the resonance condition of 3D-RCE [9,13]. In other words, for the transition energy  $\Delta E$ ,

$$\begin{aligned} \Delta E &= h\gamma\mathbf{g}_{k,l,m} \cdot \mathbf{v} \\ &= \frac{h\gamma v}{a} \{\sqrt{2}(k \cos\phi + m \sin\phi) \cos\theta + l \sin\theta\}, \quad (1) \end{aligned}$$

where  $h$  is Planck's constant and  $\gamma$  is the Lorentz factor.

The experiment was performed at the heavy ion medical accelerator in Chiba (HIMAC) [11]. Heliumlike  $\text{Ar}^{16+}$  and  $\text{Fe}^{24+}$  ions were accelerated to 416 and 423 MeV/u, respectively, and passed through a thin Si single crystal after collimation by a hole of diameter 0.6 mm. The path length in the crystal was 1.0  $\mu\text{m}$ . Three-dimensional RCE from  $1s^2$  ( $^1S$ ) to  $1s2p$  ( $^1P$ ) was observed through the detection of the deexcitation  $K\alpha$  x rays from the ions by two Si(Li) detectors, which were typically placed 180 mm away from the crystal. The  $K\alpha$  x rays were emitted only through the excitation of the  $K$ -shell electron, because the electron capture cross section was negligibly small in the present high-energy region. The two detectors were placed at  $41^\circ$  with respect to the ion beam in the horizontal and vertical planes, i.e., the  $y$ - $z$  and  $x$ - $z$  planes, as shown schematically in Fig. 1(b). In the ion rest frame, taking into account the Lorentz transformation, the detection angles were almost  $90^\circ$ . Reflecting the electric dipole radiation character, the Si(Li) detector placed on the vertical plane detected the  $K\alpha$  x rays from the  $1s2p_y$  and  $1s2p_z$  substates. The horizontal detector observed the deexcitation of the  $1s2p_x$  and  $1s2p_z$  substates. This allowed us to determine the alignment direction of the ions from the ratio of intensities in the two directions.

We measured the x-ray yields under the single and double resonance conditions of 3D-RCE. Under the single resonance condition to the  $1s2p$  state, we examined the  $\mathbf{g}_{k,l,m}$  dependence of the x-ray emission direction. Hereafter, we refer to a component of the oscillating field specified by  $\mathbf{g}_{k,l,m}$  as a  $\mathbf{g}_{k,l,m}$  component. When we scanned the tilt angle  $\theta$  at a fixed  $\phi$ , the resonance condition of Eq. (1) was satisfied at the different angles of  $\theta$  for each  $\mathbf{g}_{k,l,m}$ . Figure 2(a) and 2(b) show the  $K\alpha$  x-ray yields from  $\text{Ar}^{16+}$  and  $\text{Fe}^{24+}$  as a function of the transition energies, converted from the tilt angle  $\theta$  using Eq. (1). The energy differences between the  $1s^2$  and  $1s2p$  states were 3139.55 eV and 6700.41 eV for  $\text{Ar}^{16+}$  and  $\text{Fe}^{24+}$  [14],

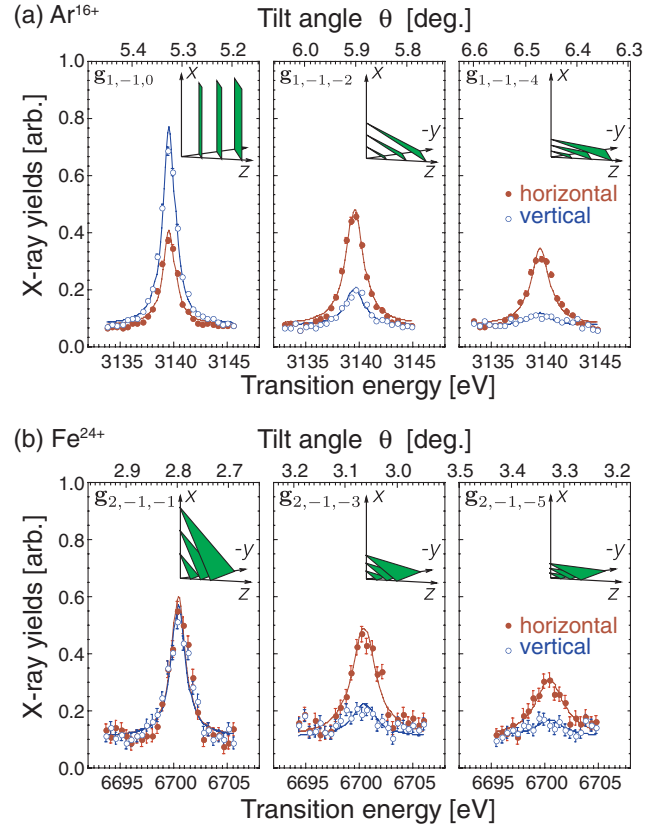


FIG. 2 (color online). (a) The  $K\alpha$  x-ray yields from 416 MeV/u  $\text{Ar}^{16+}$  in the horizontal ( $\circ$ ) and vertical ( $\bullet$ ) directions, excited by the  $\mathbf{g}_{1,-1,0}$ ,  $\mathbf{g}_{1,-1,-2}$ , and  $\mathbf{g}_{1,-1,-4}$  components, respectively. Corresponding arrays of atomic planes are shown in the insets. The transition energy was scanned by tilting  $\theta$  at  $\phi = -0.23^\circ$ . (b) The  $K\alpha$  x-ray yields from 423 MeV/u  $\text{Fe}^{24+}$  excited by the  $\mathbf{g}_{2,-1,-1}$ ,  $\mathbf{g}_{2,-1,-3}$ , and  $\mathbf{g}_{2,-1,-5}$  components, respectively, at  $\phi = -0.11^\circ$ . The solid lines are the fitted curves. The angles  $\phi$  were selected to be enough larger than the critical angle for planar channeling ( $0.0095^\circ$ ).

respectively. The relative detection efficiency of the two detectors was calibrated assuming the absence of anisotropy in the  $K\alpha$  x-ray emission under the nonresonant condition. In Fig. 2(a), when the  $\text{Ar}^{16+}$  ions were excited by the  $\mathbf{g}_{1,-1,0}$  component, the x-ray emission in the vertical direction was twice as intense as that in the horizontal direction. In contrast, for excitation by the  $\mathbf{g}_{1,-1,-2}$  component, the vertical x-ray yield was significantly smaller than the horizontal one. In the case of the  $\mathbf{g}_{1,-1,-4}$  component, the x rays were observed mostly in the horizontal direction, which indicated the selective population of the  $1s2p_x$  magnetic substate. Evidently, the alignment direction approached the  $x$  direction with increases in  $|m|$ , as expected from the direction of atomic planes, which is shown schematically in the insets of Fig. 2. In the case of the  $\text{Fe}^{24+}$  ions [Fig. 2(b)] excited by the  $\mathbf{g}_{2,-1,-1}$  component, the x-ray emission yields were almost identical in both directions. As in the  $\text{Ar}^{16+}$  case, the x-ray emission from  $\text{Fe}^{24+}$  ions became dominant in the hori-

zontal direction as  $|m|$  increased. Note that the resonance widths originate not only from coherence relaxation but also from the non-negligible velocity distribution and beam divergence [9]. Equation (1) indicates that the contribution of the beam divergence  $\Delta\phi$  should increase with the Miller index  $|m|$ , which is reflected in the spectra.

We estimated the vertical to horizontal ratios ( $V/H$  ratios) of the x-ray yield from the probability of excitation to each magnetic substate. The probability of the electric dipole transition is determined by the squared transition matrix element  $|\langle 1s2p | \mathbf{F}'_{\mathbf{g}} \cdot \mathbf{d} | 1s^2 \rangle|^2$ , where  $\mathbf{d}$  is the dipole operator and  $2\mathbf{F}'_{\mathbf{g}}$  is the amplitude of the oscillating field in the ion rest frame. When we take the  $2p_x$ ,  $2p_y$ , and  $2p_z$  wave functions as a basis of the ionic  $2p$  state, the probabilities of excitation to the  $1s2p_x$ ,  $1s2p_y$ , and  $1s2p_z$  states are proportional to  $|F'_{g_x}|^2$ ,  $|F'_{g_y}|^2$ , and  $|F'_{g_z}|^2$ , respectively, because the oscillating field is linearly polarized. By the Lorentz transformation of the electric field  $\mathbf{F}(\mathbf{r})$  to the ion rest frame,  $\mathbf{F}'_{\mathbf{g}}$  reduces to  $(F'_{g_x}, F'_{g_y}, F'_{g_z}) = 2\pi V_{\mathbf{g}}(\gamma g_x, \gamma g_y, g_z)$ . Therefore, in the geometric layout of the present experiment, we expect the  $V/H$  ratio to be  $(|\gamma g_y|^2 + |g_z|^2)/(|\gamma g_x|^2 + |g_z|^2)$ . The Fourier coefficient  $V_{\mathbf{g}}$  was calculated using the Molière approximation to the Thomas Fermi potential. The effect of the lattice vibration was taken into account through the Debye-Waller factor. The squared amplitudes  $|2\mathbf{F}'_{\mathbf{g}}|^2$  in the ion rest frame are shown in Fig. 3(a) as the summation of  $|2F'_{g_x}|^2$ ,  $|2F'_{g_y}|^2$ , and  $|2F'_{g_z}|^2$ . The calculated  $V/H$  ratios are summarized in Fig. 3(b), with the experimental values obtained by fitting the observed spectra to a Lorentzian function, where the uncertainties come from the normalization and fitting procedures. These estimates reproduced the experimental results of the  $V/H$  ratios closely, clearly demonstrating that the ions were aligned to a specific magnetic substate, whose direction was properly described by the polarization

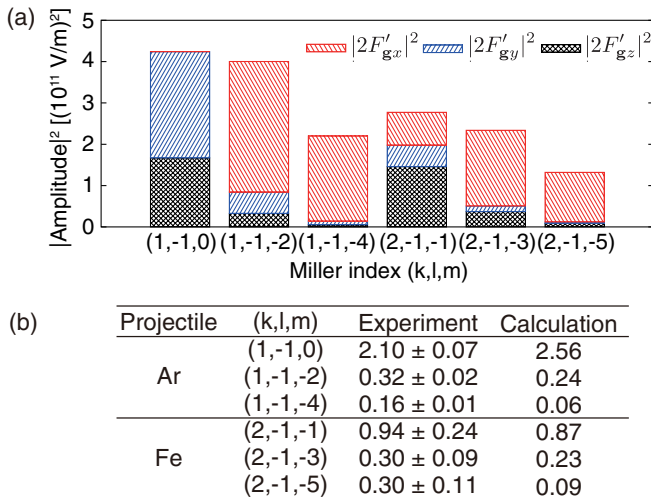


FIG. 3 (color online). (a) The squared amplitude of the oscillating field in the ion rest frame. (b) The experimental and calculated values of the  $V/H$  ratio.

direction of the oscillating field. Overall, however, the observed anisotropy was slightly smaller than the estimate (the  $V/H$  ratio is closer to unity). This can be explained by the relaxation of alignment due to collisions with target atoms in the crystal. We also compared the relative intensities of the x-ray emission among the different  $\mathbf{g}_{k,l,m}$  with the calculation. The experimental results agreed to within 10% of the calculated  $|\mathbf{F}'_{\mathbf{g}}|^2$  of the oscillating field.

We also measured the  $K\alpha$  x-ray yields from  $\text{Ar}^{16+}$  under the  $\Lambda$ -type double resonance condition, in which two frequency components simultaneously satisfy the resonance conditions of the different transitions. In this experiment, one frequency component  $\mathbf{g}_{0,0,-2}$  coupled the  $1s2p$  ( $^1P$ ) and  $1s2s$  ( $^1S$ ) states and the other probed the transition from the  $1s^2$  ( $^1S$ ) to  $1s2p$  ( $^1P$ ) states, as shown in Fig. 4(a). When  $\cos\theta \sim 1$ , the frequency of the coupling field is independent of  $\theta$ . Then, by tilting  $\theta$ , the probing field was scanned while fixing the coupling field at the transition energy of the  $1s2p - 1s2s$  (15.03 eV;  $\phi = -0.128^\circ$ ). With this configuration, we have recently reported observation of the Autler-Townes (AT) doublet [15] with the probing field of the  $\mathbf{g}_{1,-1,-2}$  component. The doublet was associated with the strong coupling of the  $1s2p$  with  $1s2s$  state, and observed through measurement of the  $\text{Ar}^{16+}$  survival fraction after passing through the Si crystal [16]. However, we could not obtain information about the population of each magnetic substate, because the measurement of the survival fraction only reflected the population of all magnetic substates. By contrast, in the present study, we

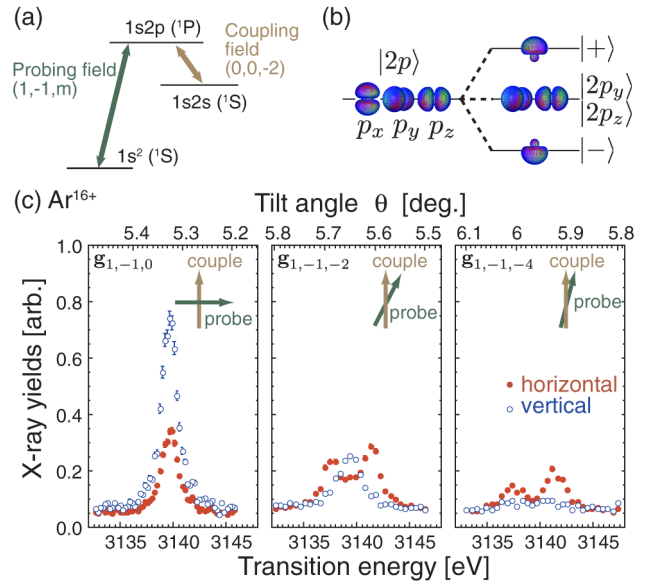


FIG. 4 (color online). (a) The  $\Lambda$ -type three-level configuration of  $\text{Ar}^{16+}$ . (b) The uncoupled (left-hand side) and the coupled (right-hand side) scheme of the probed state. (c) The  $K\alpha$  x-ray yields from 416 MeV/u  $\text{Ar}^{16+}$  in the horizontal ( $\circ$ ) and vertical ( $\bullet$ ) directions, excited by the  $\mathbf{g}_{1,-1,0}$ ,  $\mathbf{g}_{1,-1,-2}$ , and  $\mathbf{g}_{1,-1,-4}$  components, respectively, under the double resonance condition ( $\phi = -0.128^\circ$ ). The arrows indicate the polarization directions of the probing field relative to the coupling field.

can observe the x-ray emission from selective magnetic substates, i.e., specific alignment direction of the ions. Convinced by the clear demonstration of substate-selective excitation and detection technique for the single resonance, we applied this polarization-control technique to the double resonance experiment, where the polarization direction of two fields with respect to each other plays a crucial role. Figure 4(c) shows the x-ray yields from  $\text{Ar}^{16+}$  ions under the double resonance condition probed by the  $\mathbf{g}_{1,-1,0}$ ,  $\mathbf{g}_{1,-1,-2}$ , and  $\mathbf{g}_{1,-1,-4}$  components, respectively. We observed splitting of the energy level (AT doublet) only in the horizontal spectra probed by the  $\mathbf{g}_{1,-1,-2}$  and  $\mathbf{g}_{1,-1,-4}$  components, which can be interpreted as follows. Because the coupling field ( $\mathbf{g}_{0,0,-2}$  component) is polarized almost parallel to the  $x$  direction, only the  $1s2p_x$  substate is coupled with  $1s2s$ . The schematic energy levels and the shape of the wave functions are given in Fig. 4(b), where the doublet states  $|+\rangle$  and  $|-\rangle$  are the linear combinations of the  $1s2p_x$  and  $1s2s$  states. Therefore, in the case that the  $\mathbf{g}_{1,-1,0}$  component is adopted as the probing field, whose polarization direction is almost orthogonal to the coupling field, the coupled substates  $|+\rangle$  and  $|-\rangle$  are not populated. Thus, we observed a singlet resonance peak similar to that under the single resonance condition [Fig. 2(a)]. In contrast, with the  $\mathbf{g}_{1,-1,-4}$  component polarized almost parallel to the  $x$  direction, we could selectively probe the coupled substates, leading to a clear observation of the AT doublet in the horizontal direction, with no resonance peak observed in the vertical direction. In this manner, by selecting the polarization direction of the probing field with respect to the coupling field, selective probing of the coupled or uncoupled substates was demonstrated. In the case of the  $\mathbf{g}_{1,-1,-2}$  component, which has both parallel and orthogonal components to the coupling field, both coupled and uncoupled substates are simultaneously probed. Because the vertical detector selectively observed the deexcitation x rays from the uncoupled  $1s2p_y$  and  $1s2p_z$  substates, the resonance profile remained singlet. In the horizontal direction, x rays from both the coupled  $1s2p_x$  and the uncoupled  $1s2p_z$  states were observed. These anisotropic profiles of the x-ray emission provided convincing evidence for the polarization control using multiple atomic planes of the crystal.

In summary, we succeeded in controlling the population of magnetic substates by polarization control in 3D-RCE of highly charged heavy ions. The  $V/H$  ratios of the deexcitation x-ray yields from the aligned ions were well explained by the electric dipole transition. Under the double resonance condition, we demonstrated manipulation and probing of the selective magnetic substates in the three-level system. This 3D-RCE polarization-control technique opens a door to the study of quantum systems in the x-ray energy region as an alternative to the optical methods.

The authors would like to thank Professor V. V. Balashov for helpful discussions. This work was supported in part by Grants-in-Aid for Scientific Research (No. 19104010) from JSPS. Y. Nakano acknowledges support from JSPS (No. 20-10964). A.H. acknowledges support from the ‘‘Improvement of Research Environment for Young Researchers’’ program of MEXT. This experiment was one of research projects with heavy ions at NIRS-HIMAC.

\*nakano-yuji@ed.tmu.ac.jp

- [1] N. Andersen and K. Bartschat, *Polarization, Alignment, and Orientation in Atomic Collisions* (Springer, New York, 2001).
- [2] V. V. Okorokov, JETP Lett. **2**, 111 (1965).
- [3] S. Datz, C. D. Moak, O. H. Crawford, H. F. Krause, P. F. Dittner, J. Gomez del Campo, J. A. Biggerstaff, P. D. Miller, P. Hvelplund, and H. Knudsen, Phys. Rev. Lett. **40**, 843 (1978).
- [4] S. Datz, C. D. Moak, O. H. Crawford, H. F. Krause, P. D. Miller, P. F. Dittner, J. G. del Campo, J. A. Biggerstaff, H. Knudsen, and P. Hvelplund, Nucl. Instrum. Methods **170**, 15 (1980).
- [5] K. Komaki, T. Azuma, T. Ito, Y. Takabayashi, Y. Yamazaki, M. Sano, M. Torikoshi, A. Kitagawa, E. Takada, and T. Murakami, Nucl. Instrum. Methods Phys. Res., Sect. B **146**, 19 (1998).
- [6] T. Azuma, T. Ito, K. Komaki, Y. Yamazaki, M. Sano, M. Torikoshi, A. Kitagawa, E. Takada, and T. Murakami, Phys. Rev. Lett. **83**, 528 (1999).
- [7] F. J. G. de Abajo and V. H. Ponce, Adv. Quantum Chem. **46**, 65 (2004).
- [8] C. Cohen and D. Dauvergne, Nucl. Instrum. Methods Phys. Res., Sect. B **225**, 40 (2004).
- [9] C. Kondo, S. Masugi, Y. Nakano, A. Hatakeyama, T. Azuma, K. Komaki, Y. Yamazaki, T. Murakami, and E. Takada, Phys. Rev. Lett. **97**, 135503 (2006).
- [10] S. Datz, P. F. Dittner, H. F. Krause, C. R. Vane, O. H. Crawford, J. S. Forster, G. S. Ball, W. G. Davies, and J. S. Geiger, Nucl. Instrum. Methods Phys. Res., Sect. B **100**, 272 (1995).
- [11] T. Azuma, Y. Takabayashi, C. Kondo, T. Muranaka, K. Komaki, Y. Yamazaki, E. Takada, and T. Murakami, Phys. Rev. Lett. **97**, 145502 (2006).
- [12] V. V. Balashov and I. V. Bodrenko, Phys. Lett. A **352**, 129 (2006).
- [13] The extinction rule of the resonance due to the destructive interference of the oscillating field is  $k + l + m = 2j + 1$  or  $2k + l = 4j + 2$  ( $j$ : integer) for the diamond type crystals.
- [14] Yu. Ralchenko *et al.*, NIST Atomic Spectra Database version 3.0, <http://physics.nist.gov/asd3> (2006).
- [15] S. H. Autler and C. H. Townes, Phys. Rev. **100**, 703 (1955).
- [16] Y. Nakai, Y. Nakano, T. Azuma, A. Hatakeyama, C. Kondo, K. Komaki, Y. Yamazaki, E. Takada, and T. Murakami, Phys. Rev. Lett. **101**, 113201 (2008).